Lab Notes

Editors

Thomas M. Moses | Shane F. McClure
Sally Eaton-Magaña | Artitaya Homkrajae

Figure 1. This 37.41 ct rough diamond has distinct pink and colorless zones. Photos by Tebogo Hambira.

DIAMONDS

Extraordinary Large Bicolor Natural Rough Diamond

Rough pink diamonds are rarely found, and although the cause of color has been correlated with plastic deformation, the precise mechanism and atomic configuration for the resulting color are topics of continuous research. Therefore, when GIA receives a diamond with distinct pink and colorless sections (figure 1), it is of scientific interest, particularly at an astounding weight of 37.41 ct. GIA has previously examined comparable type Ia pink and colorless bicolor rough, both reportedly from Australia, in much smaller specimens weighing less than 2 ct each (Spring 2021 Lab Notes, pp. 53–55).

Sourced from the Karowe mine in Botswana, this rare find was submitted to GIA's Botswana laboratory for the GIA Diamond Origin Report service. The stone measured 24.3 × 16.0 × 14.5 mm and examination showed mostly a sharp boundary between the pink and colorless zones (figure 2).

The Karowe mine recently has been a frequent source of noteworthy diamonds, including the second-largest rough diamond ever recovered at 2,488 ct ("GIA tests the world's second largest diamond," *GIA Research News*, August 15, 2025), nine diamonds weighing more than 1,000 ct each, and several other pink diamonds, such as the 62 ct type IIa "Boitumelo" ("Lucara recovers 62 carat fancy pink diamond 'Boitumelo' from the Karowe mine in Botswana," July 13, 2021, https://lucaradiamond.com/newsroom/news-releases/lucara-recovers-62-carat-fancy-pink-diamond-boitum-122825/).

Fourier-transform infrared absorption, visible/near-infrared (Vis-NIR) absorption, and photoluminescence (PL) spectroscopy along with deep-UV imaging were collected from both the pink and the colorless portions of the submitted diamond in order to better characterize its properties. The diamond was identified as type IIa with no observable differences in the IR spectra in the two sections. Vis-NIR absorption showed the 550 nm absorption band in the spectrum collected from the pink section; unsurprisingly, it was absent from the colorless section (figure 3). There were minor differences in features detected within the PL spectra collected with 457, 633, and 830 nm lasers, along with deep-UV fluorescence imaging when comparing data collected between the pink and colorless portions. However, the full peak width at half-maximum of the H3 center (NVN^0; 503.2 nm) was significantly narrower in the pink section (0.61 nm) than in the colorless section (1.12 nm).

The 514 nm PL spectra did show some differences (figure 4). The pink zone displayed an undulating broad

Editors' note: All items were written by staff members of GIA laboratories.

GEMS & GEMOLOGY, Vol. 61, No. 3, pp. 290–301.

Figure 2. This boundary shows a sharp transition from pink to colorless zones. Photomicrograph by Wanling Tan; field of view 4 mm.

photoluminescence band centered at ~670 nm, commonly seen in the PL spectra of pink diamonds, that was not apparent in the colorless spectrum (S. Eaton-Magaña et al., "Comparison of gemological and spectroscopic features in type IIa and Ia natural pink diamonds," *Diamond and Related Materials*, Vol. 105, 2020, article no. 107784). Additionally, the 514 nm PL spectrum from the colorless zone showed a series of features from 790–840 nm; although this series of features is uncharacterized, it is often observed in the 514 nm PL spectra of rough IIa diamonds and occasionally faceted diamonds.

Nearly all natural pink diamonds derive their color from the 550 nm absorption band, which is generally accepted as a byproduct in the diamond when stress, such as mountain-building events, results in plastic deformation of the stone. From what is understood about pink diamond formation, the

Figure 3. Comparison of Vis-NIR absorption spectra collected from the pink and colorless sections. Spectra are offset vertically for clarity.

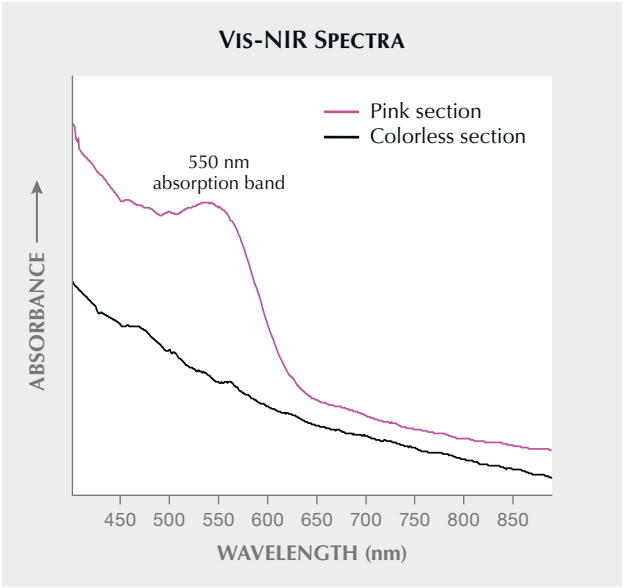

Figure 4. Comparison of 514 nm PL spectra collected at liquid nitrogen temperature from the pink and colorless sections. Spectra are offset vertically for clarity and are scaled such that the second-order diamond Raman features are equal.

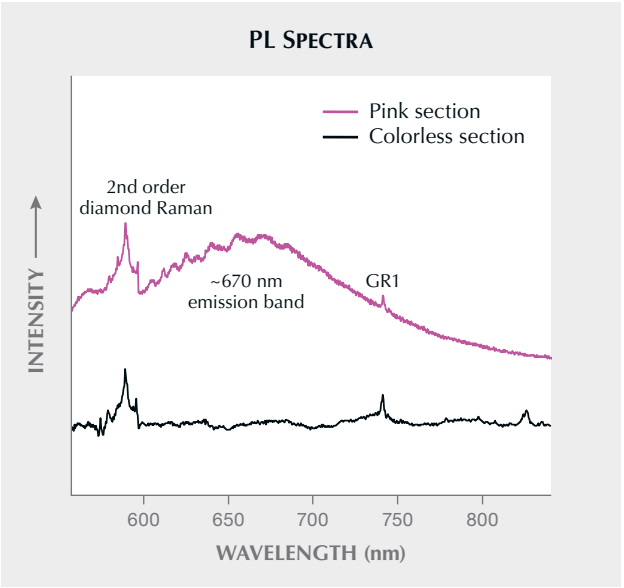

pink section likely was initially colorless and then plastically deformed resulting in its pink color; it is assumed that the colorless section formed at a later time after the stress-causing event. The distinctive appearance of this bicolor rough diamond displaying two attractive colors, its large size, and its potential to yield more information about pink diamond formation make this diamond quite noteworthy.

Sally Eaton-Magaña, Kgotlaetsho Baatshwana, and Norma-Jean Osi

Pink Diamond with Mottled Appearance

A 1.10 ct Fancy Deep brownish orangy pink round diamond was recently submitted to GIA's New York laboratory for analysis (figure 5). This diamond was multi-treated—a combination of high-pressure, high-temperature (HPHT) annealing, irradiation, and subsequent moderate temperature heating—with the intent to create nitrogen vacancy (NV) centers and thus achieve the desirable pink color. Prior to treatment, we assume this diamond was probably a less desirable brownish color (this has not been verified).

When viewed face-up, the diamond exhibited a mottled appearance. Further examination with a gemological microscope revealed that these patterns extended from a shallow depth to the polished surface. An uneven distribution of pink color created the mottled appearance—a very unusual feature for a treated pink diamond.

Figure 5. A 1.10 ct Fancy Deep brownish orangy pink diamond. Photo by Towfiq Ahmed.

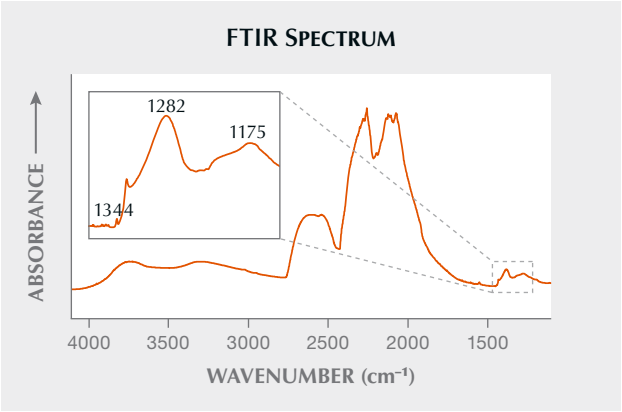

Figure 6. Mid-infrared spectrum showing the one-phonon region, A and B aggregated nitrogen at 1282 cm^{-1} and 1175 cm^{-1}, respectively, with type Ib (isolated nitrogen) at 1344 cm^{-1}.

The mid-infrared spectrum of this diamond (figure 6) shows it is a type IaAB with A aggregated nitrogen at 1282 cm^{-1} and B aggregated nitrogen at 1175 cm^{-1} distributed throughout the diamond crystal structure. Isolated single nitrogen impurities were detected at 1344 cm^{-1} (likely the result of HPHT annealing). An uneven distribution of nitrogen aggregates may have resulted in a variable NV center distribution and thus the subtle color distribution.

The visible/near-infrared (Vis-NIR) absorption spectrum obtained from this diamond has typical spectral features of a treated diamond exposed to laboratory irradiation and heat treatments. These features include the 594 nm peak indicative of irradiation, the NV^0 and NV^- centers causing the pink color, and the H2 center indicative of heat treatment (figure 7). Deep-UV fluorescence images, as observed using the DiamondView instrument, show a combination of yellow and orange fluorescence; both of these fluorescence colors can be created by NV centers and the observed color can vary

Figure 7. Vis-NIR absorption spectrum showing the 594 nm, NV^0 and NV^- (attributed to the pink color), and H2 centers, indicative of treatment.

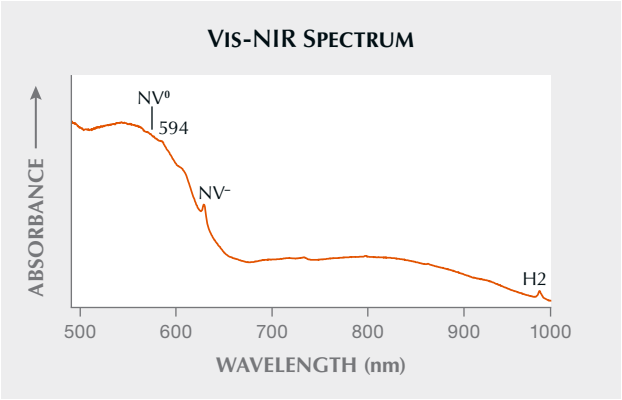

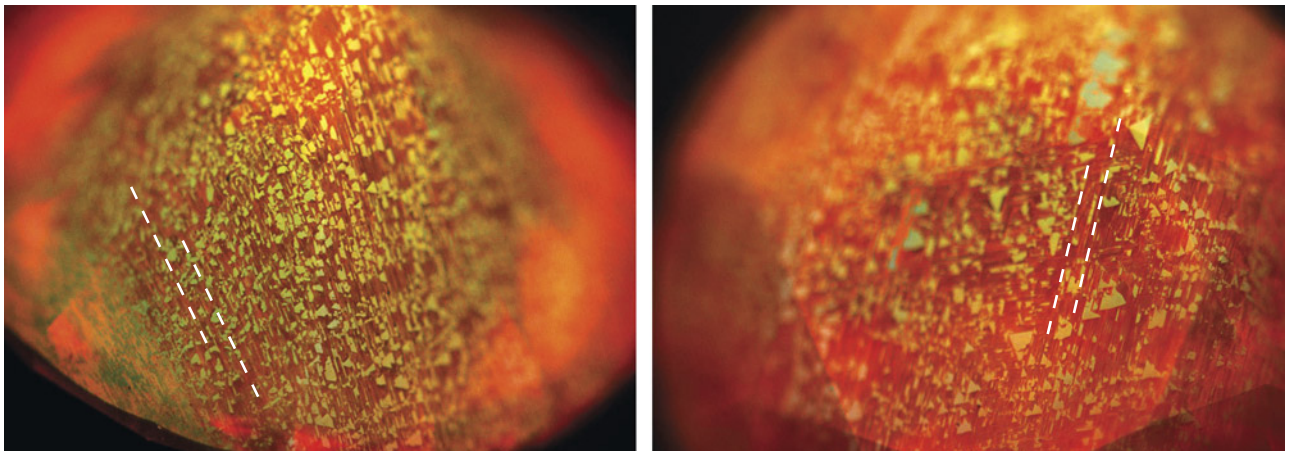

Figure 8. DiamondView images of pavilion and crown facets. The yellow and orange fluorescence, attributed to the NV^0 and NV^- nitrogen vacancy centers, follows the patterns dictated by the deformation of the crystal structure. Images by Paul Johnson.

based on the ratio of the negative to neutral NV center intensities. The NV center distribution and the variation in the ratio of the NV centers are assumed to be related to the nitrogen aggregate distribution, which could explain the mottled color distribution. However, no IR mapping to chronicle the nitrogen aggregate distribution and no photoluminescence mapping of the NV centers to confirm their distribution was performed.

After formation within the earth, the crystal structure of a diamond can be subjected to plastic deformation, which can impart a brown color to the crystal. Such deformation, which is common in brown diamonds (R. Tappert and M.C. Tappert, *Diamonds in Nature: A Guide to Rough Diamonds*, Springer, 2011), appears to resemble the fluorescence patterns observed in the DiamondView images shown in figure 8. These DiamondView images also show a striking pattern in the diamond following the deformation lines on the octahedral crystal faces. Such plastic deformation may have contributed to the mottled pattern observed on the diamond, with the nitrogen vacancy centers created by treatment appearing to follow these deformation lines.

This is a notable example of treatments used to enhance the color of a natural diamond.

Dimitry Krugolets and Paul Johnson

Starburst Cloud Inclusions in Diamond

Recently, the Carlsbad laboratory examined a 2.50 ct Faint yellow-green round brilliant diamond with several randomly distributed yellow zones consisting of stacks of clouds with four-sided star patterns near the girdle (figure 9). The clouds were clusters of micro-inclusions, with the center of each cloud containing more intensely colored particles in a cross pattern. When viewed from a different

Figure 9. Viewed through the pavilion, trails of starburst-patterned clouds were observed in patches near the girdle in a 2.50 ct diamond; in the center of each cloud were more intensely colored particles appearing to form a cross pattern. Photomicrographs by Forozan Zandi; fields of view 1.26 mm (left) and 2.34 mm (right).

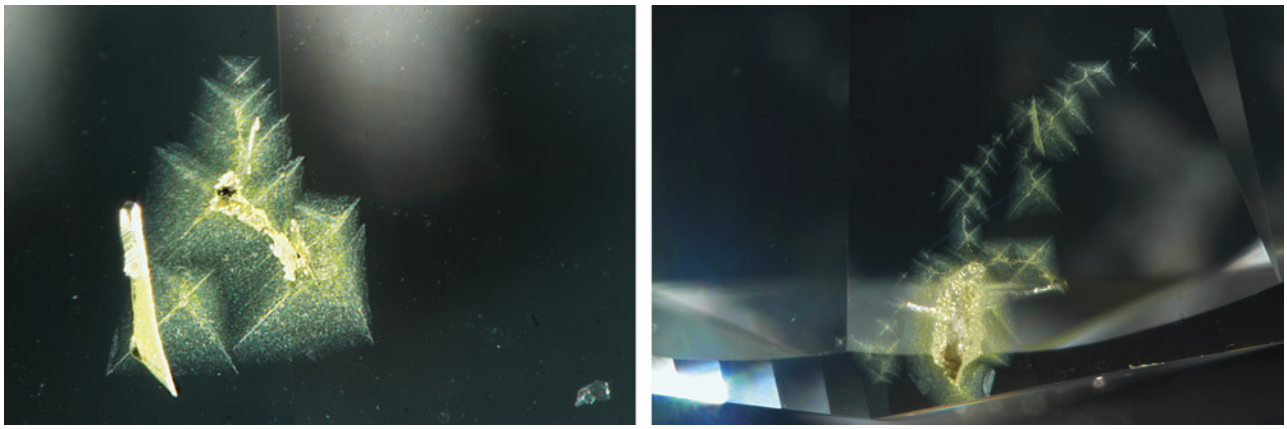

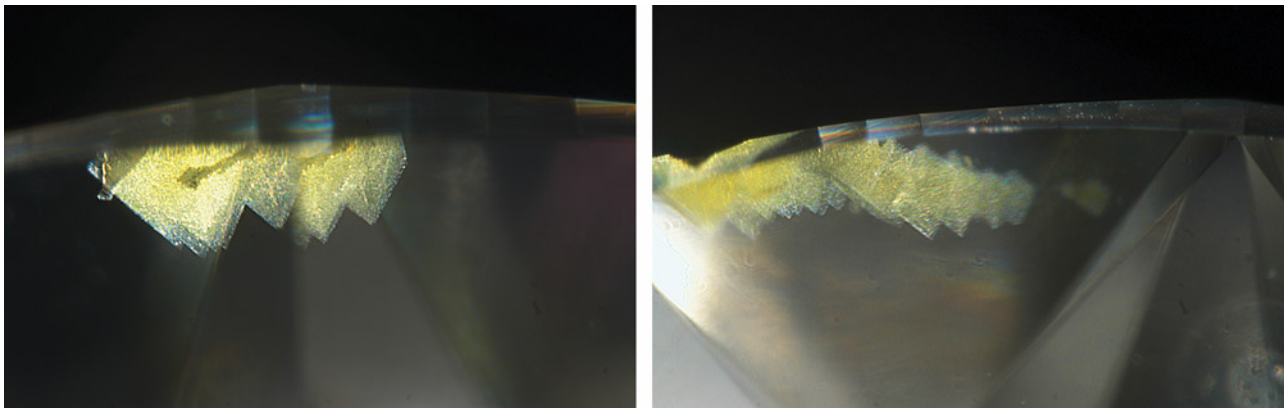

Figure 10. The same clouds appeared as a row of triangular spikes when viewed from a different direction through the pavilion. Photomicrographs by Forozan Zandi; fields of view 1.42 mm (left) and 1.58 mm (right).

direction, the same clouds appeared as a row of bright yellow overlapping triangles (figure 10). The uniqueness of these clouds triggered an in-depth investigation.

The body of the diamond exhibited blue fluorescence to long-wave (365 nm) UV radiation, and with a deep-UV (<230 nm) imaging microscope, the authors were able to discern that the cloud patches showed weak yellow fluorescence (figure 11).

The diamond's ultraviolet/visible/near-infrared absorption spectrum revealed cape absorption features at 415 (N3 center) and 478 (N2 center) nm. In addition, broad absorption bands centered at 730 and 836 nm, as well as a peak at 563 nm, were indicative of hydrogen-related defects (C.M. Breeding et al., "Naturally colored yellow and orange gem diamonds: The nitrogen factor," Summer 2020 *G&G*, pp. 194–219). The infrared absorption spectrum indicated that the diamond was type Ia with high abundance of both nitrogen and hydrogen.

Figure 11. When exposed to deep-UV excitation, the bulk of the diamond showed blue surface fluorescence, whereas the yellow color zones and the cross patterns with visibly darker particles showed weak yellow surface fluorescence. Image by Sally Eaton-Magaña.

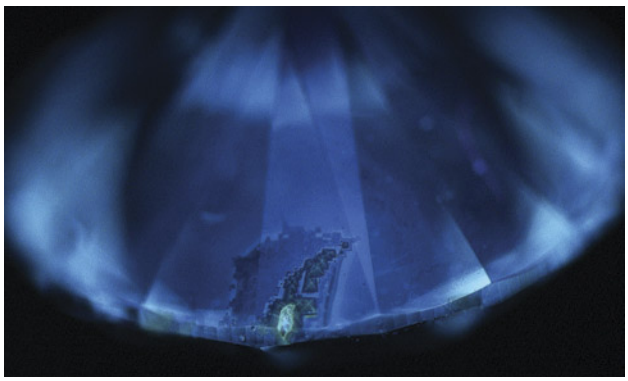

While hydrogen-related defects might cause brownish or greenish components to the diamond bodycolor, they are not responsible for the bright yellow color zones in this diamond. Generally, yellow color in diamond is caused by cape defects, H3 defects, isolated nitrogen (C-center), or a 480 nm absorption band (Breeding et al., 2020). However, patchy yellow color zones are more often associated with C-centers or a 480 nm absorption band (e.g., Breeding et al., 2020; M.Y. Lai et al., "Spectroscopic characterization of rare natural pink diamonds with yellow color zones," *Diamond and Related Materials*, Vol. 148, 2024, article no. 111428).

Photoluminescence (PL) spectra were collected on the bright yellow color zones and the surrounding areas, and neither the H3 center (at 503.2 nm) nor the characteristic PL features associated with the 480 nm absorption band (Lai et al., 2024) were detected. This finding suggests that these were not the causes for the yellow color zones in this diamond. The NV^- center at 637 nm, a common feature of diamonds colored by isolated nitrogen, was detected only within the bright yellow color zones, indicating that the yellow color was likely due to the presence of C-centers located in a confined region on the surface of the diamond.

Previously, a yellow overgrowth layer that formed on top of a near-colorless diamond in the late stage of diamond growth was reported (e.g., M.Y. Lai et al., "Yellow diamonds with colourless cores – Evidence for episodic diamond growth beneath Chidliak and the Ekati Mine, Canada," *Mineralogy and Petrology*, Vol. 114, 2020, pp. 91–103). However, the composition and formation of the clouds of micro-inclusions coincident with the yellow color zones in this diamond are currently unclear and require further investigation. This diamond with starburst-patterned clouds and patchy yellow zones highlights the crucial role of *in situ* analytical techniques in gemstone identification, where the causes of color zones can be determined based on well-resolved spectroscopic features.

Forozan Zandi, Mei Yan Lai, and Sally Eaton-Magaña

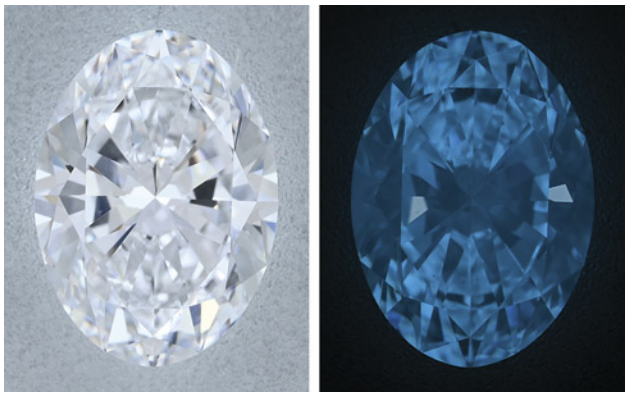

Figure 12. The 2.50 ct diamond under white LED lighting of 6500 K (left) and in a dark environment around 10 s after deep-UV excitation to showcase its phosphorescence (right). Photos by Nick "Ka Chun" Chan.

Type IIa/IaB Diamond Showing Transient Type IIb Responses

Recently, the Dubai laboratory encountered a strongly phosphorescent natural type IIa/IaB diamond, which showed a transient response, shifting to type IIb after deep-ultraviolet (<230 nm) excitation. The 2.50 ct oval-shaped diamond was graded as D color with VS_1 clarity and received Excellent grades on both polish and symmetry. Although instances of strong phosphorescence (Winter 2017 Gem News International, pp. 476–478; Summer 2021 Gem News International, pp. 177–178) and similar transient responses in natural diamonds (J. Li et al., "A diamond with a transient 2804 cm^{-1} absorption peak," *Journal of Gemmology*, Vol. 35, No. 3, 2016, pp. 248–252; Winter 2018 Gem News International, pp. 453–455) have been reported previously, this diamond's size and quality make it notable.

Strong and long-lived phosphorescence such as the blue phosphorescence observed in this diamond is typical of high-pressure, high-temperature (HPHT) laboratory-grown diamonds. As the necessary ingredients for observed phosphorescence, neutral boron and neutral isolated nitrogen can be present in HPHT-grown diamonds in abundance. However, when observed in natural diamonds, particularly those with a D color grade, phosphorescence is usually weak and fleeting. The fact that this diamond exhibited a strong and long-lasting phosphorescence (figure 12) with a duration of more than one minute prompted further investigation.

Photoluminescence (PL) spectra obtained using 830 nm laser excitation at liquid nitrogen temperature showed a very weak 883.1/884.6 nm doublet, a feature that is related to nickel impurities. In addition, 514 nm laser excitation produced a spectrum with a weak nickel-related broad band centered at ~640 nm (W. Wang et al., "Natural type Ia diamond with green-yellow color due to Ni-related defects," Fall 2007 *G&G*, pp. 240–243) and a sharp 694 nm peak ascribed to Ni-N complexes (C.M. Breeding et al., "Natural-color green diamonds: A beautiful conundrum," Spring 2018 *G&G*, pp. 2–27). These characteristics all indicated the presence of nickel, but compared to those commonly seen in HPHT-grown diamonds, the PL intensities of these nickel-related features were much lower. DiamondView imaging further ruled out the possibility of an HPHT-grown diamond due to the absence of typical growth sectors.

While possible to observe nickel impurities in natural diamonds, it is rarely coupled with strong phosphorescence, warranting a more thorough investigation. A Fourier-transform infrared (FTIR) spectrum (figure 13) was re-collected immediately after

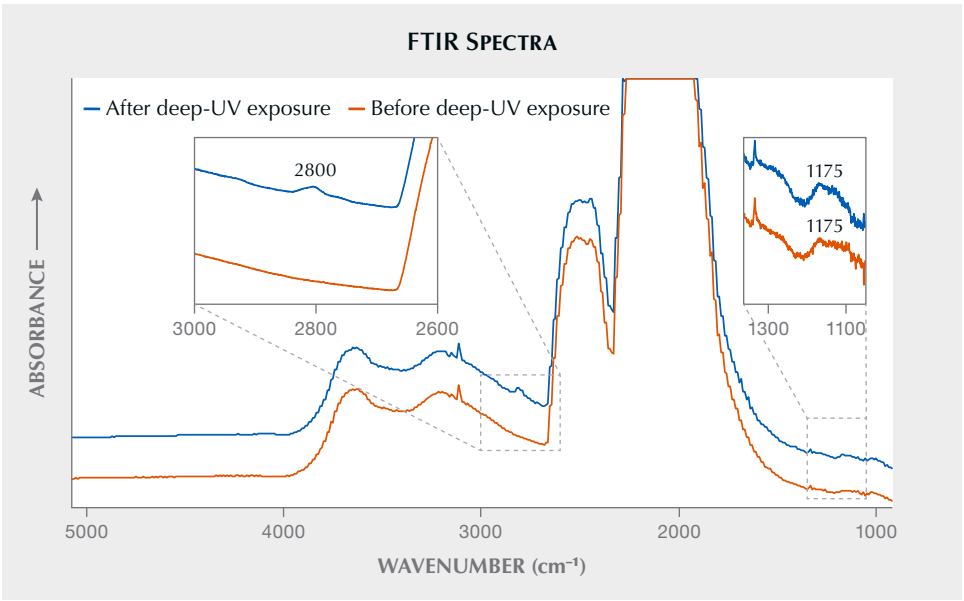

Figure 13. FTIR spectra show a change in diamond type before and after deep-UV exposure. Immediately after deep-UV exposure, an absorption at ~2800 cm^{-1} was observed, indicating an uncompensated boron concentration at ~3 ppb. Spectra are normalized for comparison and offset vertically for clarity.

deep-UV exposure. An absorption at 2800 cm^{-1} was induced which correlated to an ~3 ppb concentration of uncompensated boron, and then it slowly decayed and became undetectable within a few minutes, a timeframe longer than the duration in which observable phosphorescence dissipated. The weak nitrogen B-center at 1175 cm^{-1}, on the other hand, remained unaffected by deep-UV exposure. This transient response suggested that boron had been made uncompensated upon deep-UV exposure and then became detectable under FTIR spectroscopy. A mechanism has been suggested by Dean (P.J. Dean, "Bound excitons and donor-acceptor pairs in natural and synthetic diamond," *Physical Review*, Vol. 139, 1965, pp. A588–A602), and a decay model has also been proposed and studied (J. Zhao et al., "Phosphorescence and donor-acceptor pair recombination in laboratory-grown diamonds," *Physical Review B*, Vol. 108, 2023, article no. 165203).

For PL analysis, the sample was transferred immediately after deep-UV exposure to the PL system. Each PL spectrum was re-collected shortly after deep-UV exposure, but no noticeable changes were seen before and after deep-UV irradiation. Unlike typical type IIb natural diamonds, there were no detectable 648.2 cm^{-1}, 3H, or other characteristic type IIb emissions.

This example demonstrates the intertwined relationships and complexity of features observed in both natural and laboratory-grown diamonds. Reliance on a single observable screening feature such as strong phosphorescence might lead to misidentification. Advanced gemological testing and thorough identification processes are fundamentally important to ensure an accurate gem identification result.

Nick "Ka Chun" Chan and Satyaprasad Pradhan

Prismatic Bicolor DUMORTIERITE Crystal

Dumortierite is an orthorhombic, fibrous aluminum borosilicate mineral ($Al_7BO_3(SiO_4)_3O_3$) that typically forms slender prismatic crystals with spectacular color and pleochroism. The crystals can vary in color from brown, blue, and green to rarer violet and pink. These color variations are caused by the substitution of iron and other trivalent elements for aluminum. Dumortierite typically occurs in high-temperature, aluminum-rich regional metamorphic rocks resulting from contact metamorphism as well as in boron-rich pegmatites, with several reported sources, including Austria, the United States (Nevada), Madagascar, and Russia. A few reports of the mineral's occurrence have been published in the literature, which may be of general interest to mineralogists (e.g., A.B. Peck, "Dumortierite as a commercial mineral," *American Mineralogist*, Vol. 11, No. 4, 1926, pp. 96–101). Because perfect dumortierite crystals are very rare, small crystals surrounded by quartz and andalusite are more typically observed. Dumortierite has been reported to commonly occur as a blue mineral inclusion in quartzite (Spring 2015 Gem News International, pp. 100–102).

Recently, GIA's Bangkok laboratory received a 63.17 ct partially polished rough crystal with a prismatic shape and hexagonal cross section, measuring approximately 26.70 × 17.24 × 15.23 mm. The sample exhibited a uniform gray-blue color externally, with a strongly zoned bicolor core running along the length of the crystal featuring a pinkish orange center surrounded by a rim of gray-blue (figure 14). The color zoning was reminiscent of watermelon tourmaline's appearance, but in a different crystal form and color. The bicolored zoning observed in this dumortierite may be the result of a change in trace element composition during the crystal's growth.

Figure 14. A 63.17 ct (26.70 × 17.24 × 15.23 mm) prismatic bicolor dumortierite rough crystal, viewed from the side (left) along with a cross-section view (right), displaying a pinkish orange core and a gray-blue outer layer. Photos by Lhapsin Nillapat.

A refractive index of 1.67–1.69, a hydrostatic specific gravity of 3.38, and Raman spectroscopy identified this stone as dumortierite. The stone displayed strong chalky green fluorescence throughout the surface under short-wave (254 nm) ultraviolet radiation. Microscopic observation revealed a strong, partially hexagonal growth feature along the crystal outline with a zoned pinkish orange core and a gray-blue outer layer. The partially hexagonal polished cross section displayed triangular sectors under cross-polarizing filters. Fluid inclusions and fingerprints as well as intersecting cleavage planes were also present in the stone.

As the cause of blue color in dumortierite has been previously reported to be mainly from Fe^{2+}-Ti^{4+} intervalence charge transfer (A.N. Platonov et al., "Fe^{2+}-Ti^{4+} charge-transfer in dumortierite," *European Journal of Mineralogy*, Vol. 12, No. 3, 2000, pp. 521–528), energy dispersive X-ray fluorescence was also performed on the stone to obtain elemental information and to support its identification. High aluminum and silicon, which are among the main components of dumortierite, were detected along with small peaks of other elements, such as silver, titanium, chromium, and iron.

This dumortierite rough crystal is remarkable for its vivid, clearly separated bicolor zones and its rarity, and to the author's knowledge, is the most significant example reported in the literature due to its size, color, and shape.

Ungkhana Atikarnsakul

Figure 15. Face-up appearance of a quench-crackled and dyed laboratory-grown colorless sapphire, measuring 13.10 × 12.73 × 7.51 mm. Photo by Adriana Gudino.

Quench-Crackled and Dyed LABORATORY-GROWN SAPPHIRE

One common process used to alter gemstones is the "quench-crackle and dye" treatment, in which a heated stone is quenched in room-temperature water, inducing fractures that allow dye to penetrate the stone and change the appearance of its color. This technique was introduced in the 1990s (S.F. McClure and C.P. Smith, "Gemstone enhancement and detection in the 1990s," Winter 2000 *G&G*, pp. 336–359) and is typically applied to quartz, cubic zirconia, glass, and other synthetic gemstones due to their low cost and high availability.

The Carlsbad laboratory recently received a 12.65 ct laboratory-grown colorless sapphire that showed signs of treatment (figure 15). At first glance, the overall face-up color of this stone suggested it was a Paraíba tourmaline or a low-quality emerald. With the unaided eye, the color-causing dye-filled fractures were faintly visible. The refractive index, specific gravity, and other basic gemological tests identified the material as sapphire. Along with the lack of natural inclusions, testing with X-ray fluorescence revealed the absence of both gallium and iron, confirming that the stone was laboratory-grown. Visible/near-infrared (Vis-NIR) absorption spectroscopy displayed a broad band around 650 nm that did not match natural color-causing components found in corundum (figure 16). This explains the unnatural color of this sapphire. With a microscope, the fractures within this stone displayed characteristic weblike fractures induced by quenching. Unlike naturally occurring fractures, the fractures

Figure 16. A comparison of the Vis-NIR spectra of a natural colorless sapphire, a natural bluish green sapphire, and the bluish green laboratory-grown sapphire demonstrates that the color in the latter results from the dye seen in figure 17. Spectra are offset vertically for clarity.

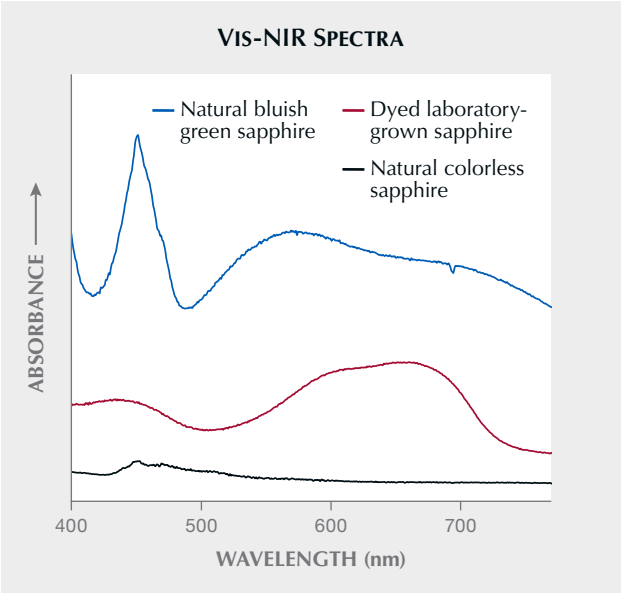

Figure 17. Dye concentrations along shallow, weblike induced fractures evenly spaced across the surface of a colorless laboratory-grown sapphire. Photomicrograph by Jamie Price; field of view 5.50 mm.

produced by this type of treatment have uniform spacing and depth, as shown in figure 17.

Jamie Leigh Price

PEARLS

Two Assembled Pearls

Recently, GIA's Mumbai laboratory received an intriguing pair of mounted pearl earrings, which were later unmounted for identification and concluded as assembled pearls. Both button-shaped pearls were partially drilled and exhibited a light cream hue. Pearl A measured 12.19 × 11.88 × 7.38 mm and weighed 7.40 ct, and pearl B measured 12.58 × 12.06 × 9.18 mm and weighed 9.37 ct (figure 18).

The face of each pearl appeared smooth and showed typical fine overlapping aragonite platelets, while each base exhibited prominent layering of materials used in the assembly process. The inner layers revealed a concentric acicular core with significant cracks typically seen in a natural pearl growth structure. This was surrounded by a layer of yellowish translucent material consisting of brown bubble-like spots, likely the adhesive material used in bonding the inner core with the outer nacreous dome (figure 19).

Real-time X-ray microradiography (RTX) imaging of the two pearls revealed similar unusual internal compositions (figure 20). The inner cores were distinctly rounded and exhibited growth features consistent with those of natural pearl. The outer domes appeared more button shaped, featuring a straight profile that flared outward toward the base and lacked a defined growth structure. These features suggested they may be blister materials, as indicated by the visible dark conchiolin layer and open skirts. However, whether these nacre domes were shell blisters, blister pearls, or cut whole pearls, and whether they were naturally formed or cultured could not be determined.

Figure 18. Two partially drilled button-shaped light cream assembled pearls weighing 7.40 and 9.37 ct, respectively, mounted in a pair of earrings. Photo by Gaurav Bera.

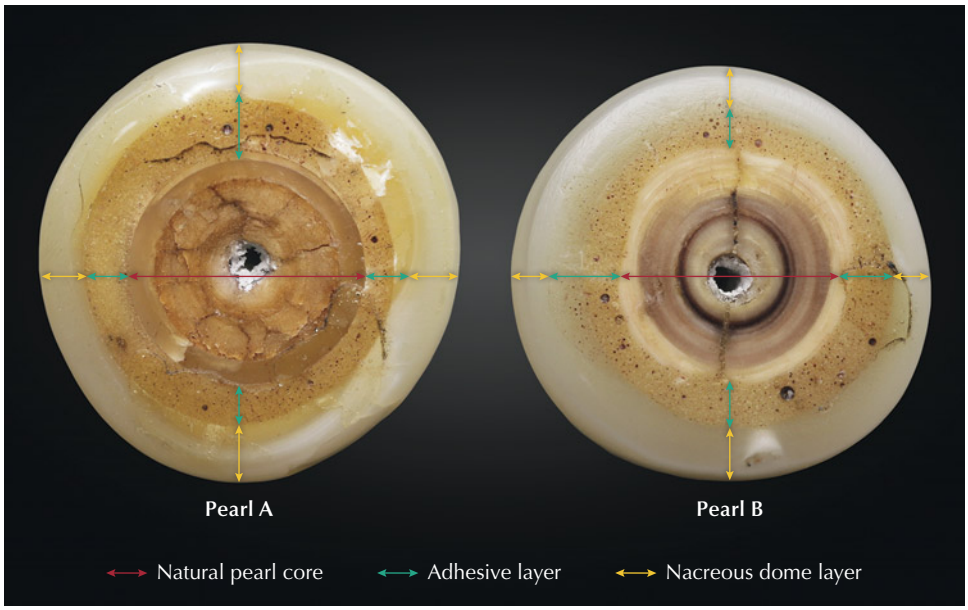

Figure 19. The base of pearl A measuring 12.19 × 11.88 mm and pearl B measuring 12.58 × 12.06 mm, showing the layering of different materials used in the assembly process. Photos by Gaurav Bera.

Therefore, their exact identity remains inconclusive (Fall 2015 Lab Notes, p. 318). Notably, each pearl showed a wide opening at the end of its drill hole. RTX imaging indicated that pearl A was partially drilled and pearl B was fully drilled prior to assembly. Both surface evidence and RTX imaging suggest that these natural cores had been bonded with the nacre domes using a radiolucent adhesive material. The natural cores and nacre domes may or may not belong to the same pearl. In addition, both pearls presented a significant internal void, which is a typical characteristic of assembled pearls or materials such as mabe pearl.

When exposed to X-ray fluorescence, the faces of the pearls displayed a very weak greenish reaction, while the bases showed a weak greenish yellow reaction for the outer nacre domes and the inner cores remained inert. Energy-dispersive X-ray fluorescence analysis on the face of each pearl revealed no trace of manganese and high strontium levels of 1353 ppm and 1532 ppm, respectively, indicating a saltwater origin. Under long-wave (365 nm) ultraviolet radiation, the top surface of both pearls exhibited a moderate bluish reaction, while the inner bottom layers displayed a weak yellowish green to light orangy red. A weaker overall reaction was observed under short-wave (254 nm) ultraviolet radiation.

The specific type of assembled pearl observed in this pair of earrings, in which natural pearl cores are used to simulate the appearance of natural pearl growth, is uncommon. Such items require comprehensive laboratory testing for accurate identification, as once mounted, these assembled pearls can easily deceive the human eye.

Roxane Bhot Jain, Abeer Al-Alawi, and Chunhui Zhou

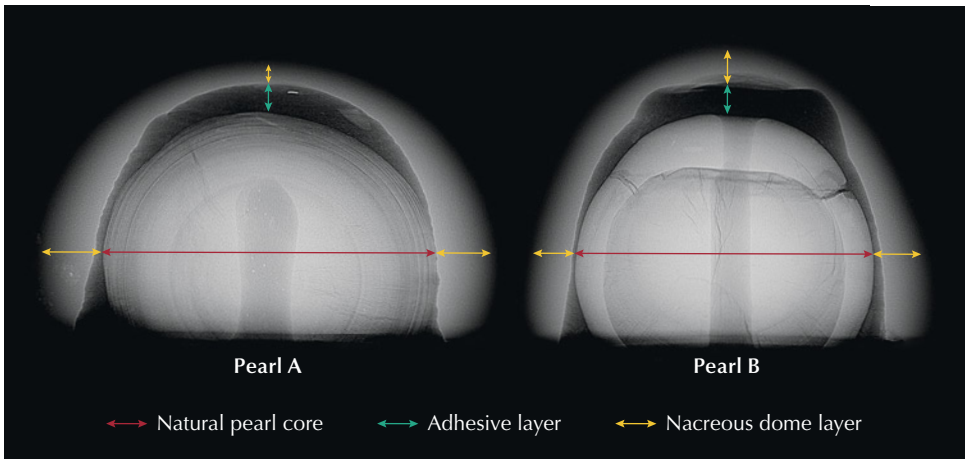

Figure 20. RTX imaging of both pearls revealing natural pearl cores (indicated by red arrows), void formations along with the radiolucent adhesive material (green arrows), and button-shaped nacreous domes (yellow arrows).

Figure 21. A dark gray and brown hollow natural pearl (2.89 ct, 11.13 × 10.47 × 10.16 mm) with a surface opening (indicated with arrow). The four fragments next to the pearl were recovered from its opening. Photos by Gaurav Bera.

Low-Heft Hollow Natural Pearl with an Opening

Pearls with low heft are always of interest as they usually exhibit a large size relative to their weight, and it is often difficult to ascertain whether they are hollow or have been filled. GIA's Mumbai laboratory recently received for identification a dark gray and brown semi-baroque pearl weighing 2.89 ct and measuring 11.13 × 10.47 × 10.16 mm (figure 21). Chemical analysis using energy-dispersive X-ray fluorescence determined no measurable manganese but a strontium content of 934 ppm, indicating a saltwater origin. Under long-wave (365 nm) and short-wave (254 nm) ultraviolet radiation, the pearl was inert.

The pearl contained a surface opening measuring approximately 2.46 × 1.94 mm, forming a window into the pearl where light brown fragments could be observed (figure 22, left). During transport and through the course of testing, four angular-shaped fragments with slightly rounded edges emerged from the opening, each weighing approximately 0.01 ct (figure 22, right), suggesting they had fractured within the pearl.

Real-time X-ray microradiography (RTX) revealed a large void with a dark gray radiolucent material inside, surrounded by a lighter gray outer rim of nacre (figure 23, left). The structure was more apparent using X-ray

Figure 22. Left: Opening in the pearl's surface with fragments visible. Right: A fragment that was dislodged from the pearl. Photomicrographs by Keaton Talker; fields of view 6.40 mm (left) and 3.00 mm (right).

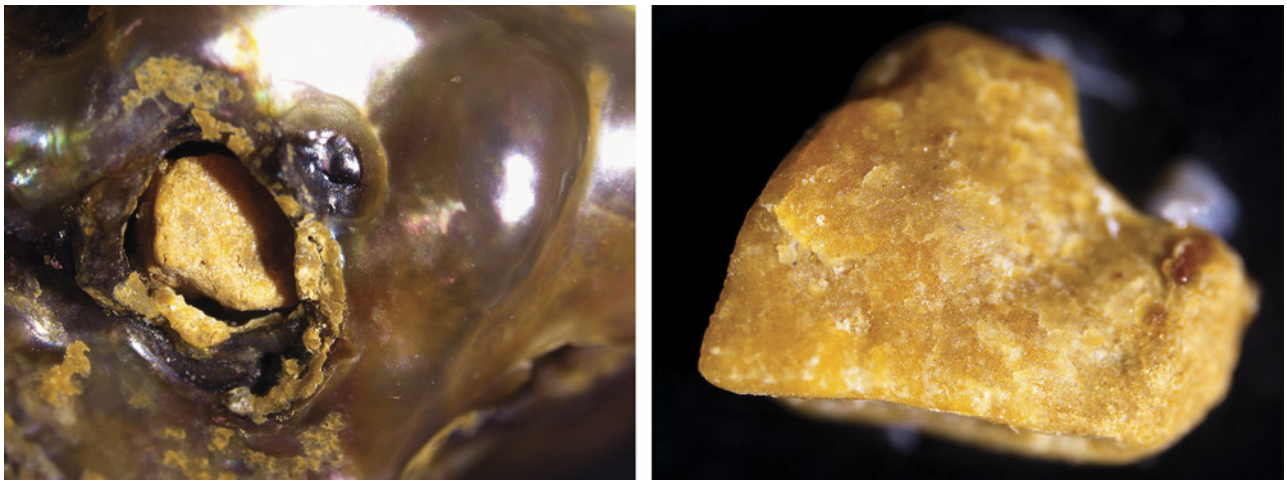

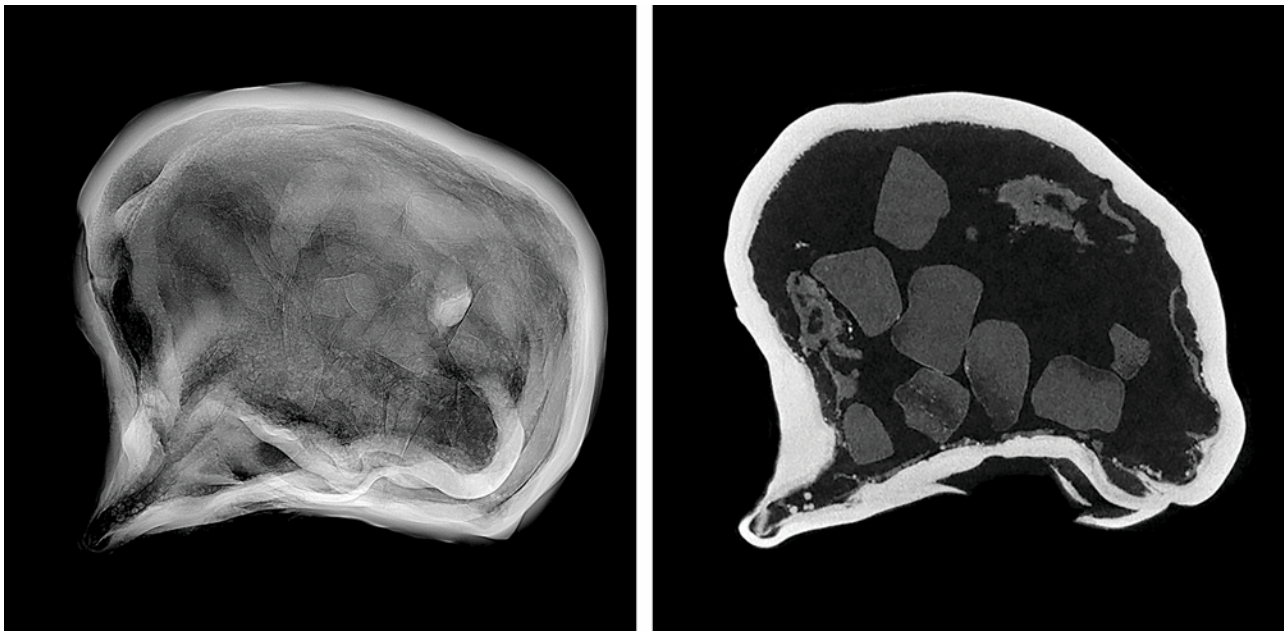

Figure 23. RTX image (left) and µ-CT image (right) of the 2.89 ct pearl with faint radiolucent material visible in the hollow void.

computed microtomography (µ-CT) imaging (figure 23, right), where many radiolucent fragments were visible inside the large void.

Further microscopic observation suggested that the dislodged fragments were made of an organic-rich resinous substance that appeared brownish yellow, similar to the fragments inside the opening and the organic material around it. However, due to the fragile nature of the pearl, Raman spectroscopy to conclusively identify this material was not possible.

Although some hollow pearls are intentionally filled with foreign materials to increase their weight and durability (Summer 2019 Lab Notes, pp. 251–254), the material inside this pearl appeared to be an organic-rich substance that naturally formed within the pearl. In addition, the void's shape followed the outline of the pearl, which has been previously observed in natural pearls ("Pearls with unpleasant odors," *GIA Research News*, March 23, 2009). The opening on the pearl's surface provided a rare glimpse into its natural filling, allowing the observation of organic-rich material as it became dislodged—a fascinating and significant occurrence.

Nishka Vaz and Abeer Al-Alawi